A Critical Review of the State-of-the-Art in the Performance of Applied-field Magnetoplasmadynamic Thrusters

A.D. Kodys*and E.Y. Choueiri†
Electric Propulsion and Plasma Dynamics Laboratory(EPPDyL)
Princeton University, Princeton, New Jersey 08544

AIAA-2005-4247‡

July 11-13, 2005

Abstract

A critical state-of-the-art (SOA) review of the performance of applied-field magnetoplasmadynamic thrusters (AF-MPDT) operating with various propellants, including lithium, is presented. The measured performance of the thrusters is critically evaluated and compared using several non-dimensional parameters. The best available performance (50-69% thrust efficiency and specific impulses in the 4000-5500 s range) was obtained at 20 kW with lithium propellant. At the higher power levels ($\sim$ 200-500 kW) of relevance to proposed nuclear planetary missions and solar lunar missions, the best performance to date was obtained with the Moscow Aviation Institute's 200-kW lithium thruster (MAI 200kW): P=185 kW, η=50% and I_{sp}=4240 s (not including power to the solenoid or lithium vaporizer). The MAI 200kW is the only thruster, for which reliable performance data was found, to operate in this power range. High facility background pressures (above 0.1-1.0 mTorr) are shown to invalidate much of the existing gas-fed AF-MPDT performance measurements. The only AF-MPDT data obtained at background pressures below 0.1 mTorr in the literature reviewed were obtained either by using condensable vapor propellants (mainly lithium) or by operating in quasi-steady mode.

1 Introduction

The applied-field magnetoplasmadynamic thruster (AF-MPDT) is a high thrust density, hybrid plasma accelerator which operates in the moderate power range of 10s to 100s of kW. The AF-MPDT has the potential of providing specific impulses (I_{sp}) of 5000-6000 s and thrust efficiencies (η) greater than 50% at power levels between where low power ($\lesssim$10s kW) Hall accelerators and high power ($\gtrsim$ 500 kW) self-field MPDTs (SF-MPDTs) have been optimized.

Much experimental and theoretical work has been done concerning AF-MPDTs since the early 1960s. The resulting thruster designs, operating regimes, optimization hypotheses and the quality of data produced have been as varied as the groups which have produced them. Thruster powers from 2 kW to 4 MW (50-18,000 A) have been investigated at applied field strengths up to 0.6 T and propellant flow rates from 0.9 mg/s to 4.5 g/s. Argon, hydrogen, and lithium have been the most popular propellant choices, although a significant amount of data has also been obtained using ammonia, nitrogen, helium, and cesium. Typical performance is in the 2000-6000 s I_{sp} range at maximum efficiencies of 30-70%.

There have been two major periods of activity in AF-MPDT research. The first coincided with the discovery of electromagnetic acceleration by Ducati in 1963 [1] and tapered off in the mid 1970s. Most of the early work in AF-MPDT research was conducted

*Graduate Student, MAE Dept., NASA Graduate Student Research Program (GSRP) and Princeton University's Program in Plasma Science and Technology (PPST)

†Chief Scientist EPPDyL, Associate Professor, MAE, Applied Physics Group. Associate Fellow, AIAA.

‡Presented at the 41^{th} AIAA/ASME/SAE/ASEE Joint Propulsion Conference, July 10-14, 2005, Tucson, AZ.

by four groups in the United States; Giannini Scientific Corporation, Electro-Optical System (EOS), AVCO Research Laboratory (AVCO-Everett), and AVCO Space Systems Division (AVSSD or AVCO-RAD). A smaller research program was undertaken at NASA-Langley and thrusters similar to the EOS and AVCO-RAD designs were tested in the low pressure facilities at NASA-Lewis (now NASA-Glenn). A complete and often cited review of this early work was completed by Nerheim and Kelly in 1967 [2][1]. From 1968 through 1975, in addition to the continuation of the research by the groups mentioned above, an ammonia AF-MPDT was developed and tested at the McDonnell Douglas Corporation [6, 7], cesium and lithium vapor thrusters were developed at the Los Alamos National Laboratory [8], [5] and an extensive AF-MPDT research program was undertaken at DFVLR-Stuttgart in Germany [9, 10]. In general, the early AF-MPDT efforts were characterized by an evolution to lower powers (less than 30 kW) to meet the spacecraft power restrictions and to alkali vapor propellants to reduce pumping requirements and to increase efficiency by minimizing ionization losses.

A second period of AF-MPDT research began in the late 1980s and lasted through 1998. Valuable reviews of the work during this period have been written by Sovey and Mantenieks [11] and Krülle [9]. The focus during this period was on higher power (>100 kW) thrusters with long lifetimes suitable for planetary exploration and heavy-cargo Earth orbit missions. Significant work was conducted by Myers at NASA-Lewis (Glenn) on geometry optimization, The Moscow Aviation Institute (MAI) with lithium propellant, and at Osaka University in Japan with high power (0.5-4 MW) quasi-steady thrusters. Some low power work (< 20 kW) was conducted during this time at the University of Tokyo.

During both periods of AF-MPDT research, alkali vapor thrusters, usually operating on lithium, were popular choices. A good review of both self and applied-field alkali metal MPDT research was published by Polk and Pivirotto [12] in 1991. Applied-field work performed by several groups in the U.S. during the 1960-70s (Giannini, EOS, Los Alamos, and AVCO) was reviewed along with more recent studies in Russia. The Russian data showed good agreement with the maximum performance levels measured in the U.S. and Polk and Pivirotto concluded that alkali metal thrusters generally demonstrate better performance with less cathode wear than gas-fed thrusters[12].

In this paper we examine the previous AF-MPDT work in the context of a renewed effort in AF-MPDT research for 250-kW class thrusters. The focus is on *experimental performance* and, although much effort has gone into theoretical descriptions of the AF-MPDT, theory will only be briefly mentioned in the context of understanding the experimental data. Lifetime in AF-MPDTs will not be considered in detail here, although it remains a critical issue in MPDT (SF and AF) development. The concerns in AF-MPDTs are similar to those of SF-MPDTs and center on cathode erosion by evaporation and insulator erosion. Low power ($\sim$ 30 kW) applied-field thrusters running on ammonia [6] and lithium [13] have been operated successfully for 100 and 500 hours respectively, although significant erosion was measured. There is some evidence that a modest applied magnetic field can reduce erosion and increase lifetime in high power MPDTs[11] . Another promising path is the addition of barium to the main propellant flow to reduce cathode operating temperature[14, 13, 12]. We will not consider lifetime further in this review.

First, in Sec. 2 we present a brief description of the general AF-MPDT concept to provide a framework in which to examine the data. Existing thruster designs, operating regimes and performance characteristics are summarized in Section 3. Following a brief discussion of the effects of background pressure (Sec. 4), we will define several non-dimensional parameters to assist us in identifying trends in the available performance data in Section 5. A more detailed look at performance trends and empirical design and optimization follow in Sections 6 and 7.

2 Physical Description of the AF-MPDT

In this section we briefly introduce the general concept of the AF-MPDT and outline the basic acceleration processes and performance limits to provide a framework for the discussion to follow.

In general, the AF-MPDT[2] is a coaxial plasma ac-

[1]The MPDT work carried out at Princeton University over the past 3 decades was concerned exclusively with self-field MPDTs with the exception of the thesis work of Fradkin[3] which dealt with applied-field lithium MPDTs and whose experiments were conducted at Los Alamos National Lab[4, 5].

[2]The term Lorentz Force Accelerator (LFA) is increasingly common in MPDT literature. This nomenclature first appeared in 1991 [15] as a general term for a coaxial plasma accel-

celerator in which the azimuthal magnetic field induced by the applied current flowing between the electrodes, B_θ or B_{SF}, is augmented by an externally-generated axial field, B_A.[3] The applied field is most commonly axial within the thruster geometry and slowly diverges downstream of the main acceleration region. The addition of the applied field allows for significant propellant acceleration at current (power) levels where the induced magnetic field is weak and SF-MPDT efficiency is generally low (< 500 kW). In general the condition $B_A \gg B_{SF}$ is satisfied, although applied fields are sometimes employed at higher powers where $B_A \approx B_{SF}$. Unlike Hall thrusters, AF-MPDTs are collisional devices which typically operate at powers and flow rates 10-100 times greater than similarly sized Hall thrusters. Operation is, typically, at powers of 10s to 100s of kW with propellant flow rates in the 10s to 100s of mg/s range. The propellant can be either gaseous or metal vapor and is fed into the discharge chamber at the insulating backplate and/or through either of the electrodes. Applied fields, generated by electromagnetic coils or permanent magnets, are usually in the 0.01-0.5 T range.

The AF-MPDT is a hybrid accelerator with electromagnetic and gas dynamic processes both contributing significantly to the acceleration of the propellant. Four main acceleration modes have been identified for the AF-MPDT (for good descriptions of these modes see, for example, [9, 16]). The relative importance of each depends upon thruster design and operating conditions (current, mass flow rate, applied field strength) and the dominant/most efficient mode is still the subject of considerable debate. Briefly, the four modes are:

- **Self-field Acceleration** The applied current induces an azimuthal magnetic field which interacts with the applied current. The resulting Lorentz force density ($\boldsymbol{j} \times \boldsymbol{B}$) acts to accelerate the plasma radially inward ($j_z B_\theta$) and axially outward ($j_r B_\theta$). The axial (or blowing) component contributes directly to thrust and the radial (or pinching) component adds to the thrust indirectly through a pressure imbalance on the central electrode (cathode). The resultant thrust is proportional to J^2. This mechanism has been well described by Maecker, Jahn [17], Choueiri [18] and others but is small contribution to the total thrust at the currents usually encountered in AF-MPDTs.

- **Swirl Acceleration** The Lorentz interaction of the applied current and the applied magnetic field ($j_r B_z$, $j_z B_r$) is purely in the azimuthal direction and acts to swirl the plasma. A large fraction of the energy imparted in this way can be converted to axial energy through the expansion of the rotating plasma in a physical and/or magnetic nozzle. For the swirl mode the expected thrust scaling would be with JB_A. This scaling has often been observed experimentally and swirl acceleration is often considered to be the dominant acceleration mode in AF-MPDTs [3, 19].

- **Hall Acceleration** Under significantly strong applied magnetic fields and low mass flow rates (large hall parameters), an azimuthal current (j_θ) may be induced according to the generalized Ohm's Law. The induced current and the applied magnetic field produce pinching ($j_\theta B_z$) and blowing ($j_\theta B_r$) force density components in a similar manner to the self-field case. Unlike the self-field case, however, the direction of the force components (positive or negative thrust contribution) is not immediately clear in the general description. If this mode were to dominate we would expect to see thrust scale with B_A^2 [16]. There is still much debate concerning both the theoretical and experimental evidence for hall acceleration in the literature. For moderate applied fields and mass flow rates, it is probably a small contribution to the total thrust.

- **Gas Dynamic Acceleration** This mode contains the joule heating and expansion of the plasma in a physical and/or magnetic nozzle. The acceleration of the plasma is similar to that in an electro-thermal arcjet. For a given thruster design, we expect scaling of this mode with mass flow rate ($\dot{m}$) with only a weak dependence on current and magnetic field. The additional gas

erator. The term has evolved to refer to a specific subclass of MPDTs in U.S. literature. Namely, the LFA is a MPDT with a recessed, multi-channel hollow cathode, usually employing lithium propellant (LiLFA). The LFA or LiLFA can be either self-field (SF-LiLFA or simply LiLFA) or applied-field (AF-LiLFA). In this review, we use the more general AF-MPDT nomenclature exclusively.

[3]The coaxial geometry of the AF-MPDT lends itself the use of a cylindrical coordinate system. The positive radially direction, r, is outward from the central axis , the azimuthal direction (denoted θ) is around the central cathode, and the positive axial direction, z, is out of the thruster geometry.

dynamic thrust associated with increased surface pressure due to the electromagnetic pinching forces is usually not included here. At high mass flow rates (low I_{sp}'s) and low currents, the gas dynamic thrust is probably a considerable fraction of the total.

In a similar manner to the self-field MPDT, efficiency in the AF-MPDT is limited mainly by; ionization losses, electrode power deposition, and by the onset of severe voltage fluctuations and anode damage when a certain critical current is exceeded. Ionization losses are typically on the same order as the energy going into useful acceleration. The dominant electrode energy sink is the anode which can consume 20-80% of the input power. Both of these losses are reduced by operating at higher discharge (applied) currents. However, the ultimate current at which a MPDT (self or applied-field version) can operate is limited by voltage fluctuations which decrease performance and anode damage which decreases lifetime. Experimentally, operation at or above this critical current, referred to as the onset current (J^*), is usually accompanied by voltage oscillations on the order of 10% of the average voltage. Onset is generally associated with the excessive pinching of the plasma to the centerline and the subsequent "starvation" of the anode for charge carriers. It has been observed experimentally and theoretically that the value of J^* increases with increasing $\dot{m}$ and with decreasing B_A and decreasing thruster volume (measured in terms of the ratio of the anode to cathode radius; $\bar{R} \equiv R_a/R_c$).

3 The Thruster Designs and Operating Regimes

Figure 1 summarizes many of the various AF-MPDT designs which have been investigated (by group and PI), their key design features, and propellant(s) used. We limit ourselves here to thrusters for which some type of thrust data has been published, as this is necessary to gauge the thruster's performance. In Figs. 2 and 3, the thruster current, power, mass flow rate, applied field strength, and the facility background pressure (P_b) ranges over which each design has been operated are listed. Typical measured performance (I_{sp}, η) ranges for each design are given. In keeping with the conventions in the literature, reported power (P) is arc power only (i.e. the applied current times the discharge voltage) and does not include power to the applied magnetic field or for any propellant pre-heating. Efficiency (η) is thrust efficiency: $\eta = T^2/(2\dot{m}P)$, where T is the measured thrust, $\dot{m}$ is the propellant flow rate, and P is the arc power just described. A special note should be made of the background pressures at which most of this data have been taken. During much of the early work, background pressures in the 100-500 mT range were not uncommon. In Section 4 we discuss the possible implications of operation at background pressures above approximately 1 mTorr. For convenience, the relevant references for each thruster design and performance measurements are summarized in Table 3. As noted previously, these data represent a wide range of thruster designs, propellants, mass flow rates, power levels, and applied magnetic fields. We will briefly summarize a few key points here and defer a more detailed discussion of the performance of each thruster until Section 6.

From the existing literature, several general performance trends for AF-MPDTs can be identified:

- Applied-field thrusters operating at low powers (< 50 kW) are able to achieve performance (efficiency and specific impulse) equal to MW-class self-field thrusters, albeit with much lower thrust capability. This is because the I_{sp} can be increased by up to 60% by the addition of an axial magnetic field at constant power [11].
- Thrust is generally a linear function of discharge current and applied field strength [5, 23, 13, 56].
- An optimal applied field strength and shape exists and depends upon the thruster power, propellant, and mass flow rate [41, 57, 2].
- Lithium and hydrogen propellants have demonstrated the highest performance (η, I_{sp})[49, 12].
- A hollow cathode or multi-channel hollow cathode is preferable to a solid rod cathode [4, 58, 59].
- A substantial fraction of the plasma acceleration commonly occurs outside of the thruster geometry [9, 3, 24].
- Feeding some fraction of the propellant through the anode has been shown to improve performance [33], [11].

Efficiency versus specific impulse is plotted for the gaseous propellant (argon, hydrogen, helium, and ammonia) thrusters in Fig. 4 and for the lithium

Thruster	Group	PIs	Years	anode shape	R_a(cm)	cathode shape	R_c(cm)	Propellant injection	Propellant	NOTES
MAARC	AVCO-Everett	Patrick and Schneiderman	1966	diverging	0.79	conical	0.40	cathode base	H_2, NH_3	water-cooled
X-2C	AVCO-RAD	John and Bennett	1965-69	converging-diverging	2.23	conical	0.64	cathode base (Swirl)	H_2, He, NH_3, N_2, Ar	water-cooled
X-2-Alkali	AVCO-RAD	John and Bennett	1965-66	straight-diverging	2.23	conical	0.32	thru 3 ports in cathode tip	Cs, Li	lithium version had radiating W anode
LAJ-AF-CG	EOS	Cann	1965-67	cylindrical	1.50	conical	0.50	at anode	Li with H_2 buffer gas	radiation-cooled
LAJ-AF-2	EOS	Cann	1965-67	cylindrical	1.50	conical	0.50	at anode	Li	radiation-cooled; Tested in low pressure facility at NASA-Lewis
HC-8	Los Alamos	Fradkin, Blackstock and Stratton	1968-73	cylindrical	1.88	hollow cathode	0.95	through HC	Li	water-cooled
MAI-30kW	MAI	Tikhonov and Semenikhin	1994-98	contoured	3.50	MCHC	1.20	through HC	Li	radiation-cooled
MAI-150kW	MAI	Tikhonov and Semenikhin	1994-98	contoured	8.00	MCHC	2.25	through HC	Li	radiation-cooled
MAI-200kW	MAI	Tikhonov and Semenikhin	1994-98	contoured	8.00	MCHC	2.63	through HC	Li	radiation-cooled
MDX-7	McDonnell Douglas Corp.	Esker and Connolly	1969	diverging	3.18	conical	0.40	thru cathode ports	NH_3	radiation-cooled; Dt = 1.524 cm
MDX-4A (B)	McDonnell Douglas Corp.	Esker and Connolly	1967-69	diverging	2.54	conical	0.40	thru cathode ports	NH_3	radiation-cooled; Dt = 1.524 cm
MY-III	Osaka U.	Tahara, Kagaya, Yoshikawa	1984-97	straight-diverging	2.90	conical	0.48	50:50	H_2, N_2-$2H_2$, NH_3, Ar	water-cooled; Quasi-steady
X9	Stuttgart/ DFVLR	Krülle	1962-75	slightly diverging ring	2.00	hemispherical	0.50	at cathode base	Ar, He	water-cooled
X16	Stuttgart/ DFVLR	Krülle	1962-75	contoured lip	3.00	hollow cathode	0.60	hollow cathode and/or anode slit	Ar, Xe, Kr	throat diameter = 1.5 cm
AF100kW-(A-C)	Sverdrup/ Lewis	Myers and Mantenieks	1991-95	cylindrical	2.50 (3.81, 5.10)	hemispherical	0.64 (1.27)	50:50	H_2, Ar	water-cooled; 8 geometries tested
AF100kW-G	Sverdrup/ Lewis	Myers and Mantenieks	1991-95	cylindrical	3.81	conical	0.64	50:50	Ar	water-cooled; short cathode
10-kW	Tokyo U.	Arakawa, Kimura and Sasoh	1977-92	converging-diverging	2.20	conical	0.40	upstream of cathode at anode radius	H_2, N_2, He, Ar	water-cooled

Figure 1: Summary of Previous Applied-Field MPDT Designs

Thruster	Group	Propellant	Current (A)	Power (kW)	mass flow rate (mg/s)	Applied B (T)	Isp (s)	Eff (%)	Background Pressure (mTorr)
MAARC	AVCO-Everett	H_2, NH_3, N_2, Ar	300-1600	10-100	10-100	< 0.125	1000-4500	5-90	200
X-2C	AVO-RAD	H_2	300-1600	18-166	20-50	0.07-0.2	1240-8320	9-68	100-500
MY-III	Osaka U.	H_2, N_2-$2H_2$, Ar	3000-18000	480-3875	440-1370	0.1-0.5	1650-9410	12-47	0.0075
MY-III	Osaka U.	H_2, NH_3	3000-18000	360-3360	2750-4470	0.05-0.2	400-3300	7-43	0.0075
X16	Stuttgart	Ar, Xe, Kr	50-100	5-15	5-10	0-0.6	1530-3650	30-40	1 -50
X9	Stuttgart	Ar, He	400-1200	10-100	100-200	0-0.5	500-2200	7-33	500
AF100kW-A	Sverdrup/Lewis	H_2	750	46-83	25	0.034-0.084	2390-3700	15-20	0.5
AF100kW-A (B,C)	Sverdrup/Lewis	Ar	750-2000	15-83	25-140	0.034-0.2	800-1890	12-25	0.5
AF100kW-G	Sverdrup/Lewis	Ar	1000	69-115	100	0.03-0.17	800-1800	19-23	0.5
10-kW	Tokyo U.	H_2, N_2, He, Ar	70-400	2-16	0.9-15	0.025-0.25	790-5670	1-23	0.6-1

Figure 2: Typical Operating and Performance Ranges for Gas-Fed Thrusters from Fig. 1

Thruster	Group	Propellant	Current (A)	Power (kW)	mass flow rate (mg/s)	Applied B (T)	Isp (s)	Eff (%)	Background Pressure (Torr)
X-2-Alkali	AVCO-RAD	Li	100-200	4-7	0.9-6.7	0.1-0.2	1000-6100	7-36	1.E-04
LAJ-AF-CG	EOS	Li with H_2 buffer gas	100-300	10-25	7-12	0.1-0.26	2270-4530	10-54	1.E-04
HC-8	Los Alamos	Li	250-550	10-25	23-40	0.09-0.27	1520-2370	10-35	7.E-06
MAI-30kW	MAI	Li	400-900	10-30	14-20	0.10	1780-4080	30-42	1.E-04
MAI-150kW	MAI	Li	1200-2100	90-122	61-86	0.045-0.09	2290-3720	31-47	1.E-04
MAI-200kW	MAI	Li	2600-3800	123-186	92-128	0.045-0.09	2760-4240	35-50	1.E-04
EOS LAJ-AF-2	EOS/NASA-Lewis	Li	(250-500)	4-21	10	0.1-0.24	740-5470	7-69	5.E-06

Figure 3: Typical Operating and Performance Ranges for Alkali Vapor Thrusters from Fig. 1

thrusters in Fig. 5. Argon data at 10-100 kW and 0.03-0.2 T are shown to give efficiencies of about 5-25% at I_{sp}'s in the 700 to 1800s range. In the same I_{sp} range lithium propellant produced similar efficiencies (7-30%). However, lithium thrusters were able to obtain much higher I_{sp}'s at similar powers and applied fields. The only gas-fed thrusters which operated at I_{sp}'s comparable to the lithium thrusters operated with hydrogen. At similar powers, the hydrogen efficiencies were about 10-20% lower. Only the MW-class MY-III thruster operating on hydrogen was able to approach the efficiency of the 30 kW lithium thrusters at similar I_{sp}'s and required an order of magnitude more power to do so. Although the efficiencies are much greater for the MW-class Osaka University thruster, similarly high I_{sp}'s (up to 6000 s) were obtained with hydrogen at only 10 kW (Tokyo University). The best data point is for a lithium thruster operating at 5500 s with 69% efficiency. The power was 21 kW with a lithium flow rate of 10 mg/s and at an applied field strength of around 0.24 T. The scatter in the argon data taken by Myers at 100 kW is due to various thruster geometries which were tested. Before looking at the data in more details, it is prudent to pause here for a brief discussion of facility effects on AF-MPDT performance.

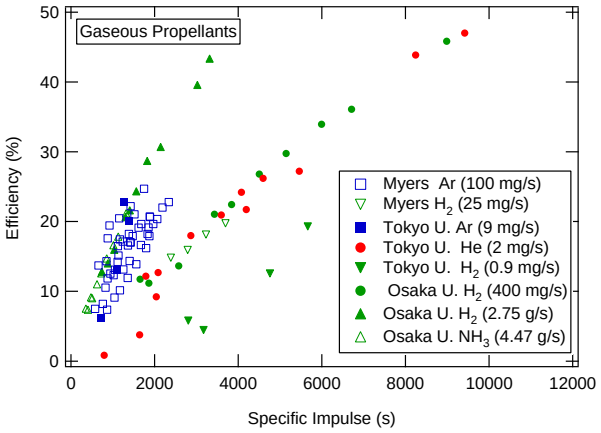

Figure 4: Efficiency versus I_{sp} for Gaseous Propellants

4 Facility Effects

No review of published data can be properly attempted without at least a mention of the conditions under which the data were obtained. The interaction of the thruster with the testing environment

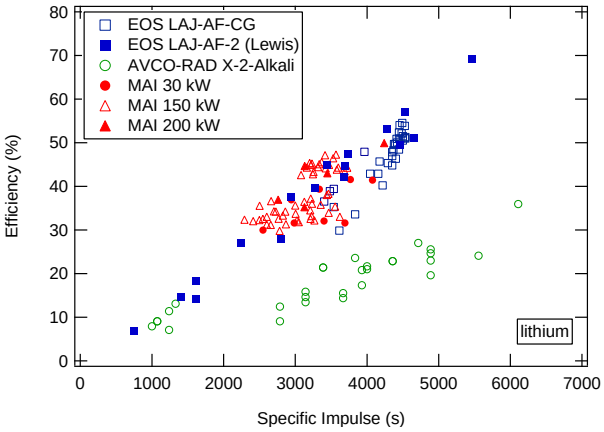

Figure 5: Efficiency versus I_{sp} for Lithium Propellant

(background pressure and wall interactions) and systematic errors in the measurements of performance parameters (due to thermal drifts, magnetic tares, probe size, etc.) can produce results that bear little resemblance to operation in the space environment. This is especially true in the case of the AF-MPDT where the propellant flow rate is usually low and the acceleration region can extend far outside the thruster geometry.

The two main measures of thruster performance, thrust efficiency (η) and specific impulse (I_{sp}), are especially sensitive to the possible entrainment of mass due to high facility pressures. Thrust efficiency ($\eta \equiv T^2/(2\dot{m}JV)$) is proportional to the square of the measured thrust (T) and inversely proportional to the input power (JV) and the metered propellant mass flow rate ($\dot{m}$). Specific impulse, $I_{sp} \equiv u_{ex}/g_o$, is usually determined by dividing the measured thrust by the propellant flow rate, $I_{sp} = T/(g_o\dot{m})$. If an unknown additional mass is present, both calculations can be in serious error.

Clearly, the definition of the proper testing environment is a critical one to AF-MPDT research. In [11], possible facility effects are shown to have clouded much of the early MPDT work in the United States. A significant blow was dealt to early, encouraging, AF-MPDT work when it was found several thrusters would operate at zero mass flow rate with similar performance to the nominal flow rate cases and no measurable erosion at background pressures as low as 1×10^{-4} Torr [23] [60].

Despite several intensive studies of background pressure effects [61, 23, 10], in which much insight has been gained, a general definition of the proper

testing environment has been elusive. Experiments have shown two possible, and competing, effects of elevated background pressure on applied-field thruster performance. First, the thrust (performance) can be degraded if a high ambient pressure interferes with the thrust mechanisms through increased collisionality [61, 10, 23] or reduced acceleration volume (i.e. plume size) [62, 2]. Second, the background gases can become accelerated by the electromagnetic body forces (especially at the lowest propellant flow rates) resulting in artificially high measured performance [23, 61, 62].

Mass flow rate, specific impulse range, and background species all appear to be important parameters in determining the effects of high P_b. At mass flow rates in the range of 10s of mg/s, Sovie and Connolly [61, 63] found that, as the background pressure was lowered, the thrust to power ratio (T/P) decreased to a minimum at around 10 mTorr and then increased again as the pressure was reduced further. The same increase in performance with reduction of P_b was observed by Cann [29]. The effect of P_b on performance was less noticeable at higher I_{sp} operation [62]. The effects of increasing P_b were found to be more pronounced when the background gases differed from the propellant gas [61, 63].

Sovie and Connolly concluded that a background pressure of less than 2×10^{-4} Torr is required to reduce facility effects to negligible levels [61, 63]. The effect of background pressure was also explored in the EOS facilities by bleeding in argon gas [29, 12]. A rough guide of $P_b \leq 10^{-3}$ Torr was established for tests with their alkali metal hall current accelerators [64, 31]. From direct Doppler shift ion velocity measurements, Krülle also concluded that $P_b < 10^{-3}$ Torr is required for accurate discharge characteristics and measurements [10]. In reviewing MPDT research through 1991, Sovey found no evidence in the literature that applied-field thruster performance was affected at background pressure below 1×10^{-4} Torr [11].

The background pressure ranges at which the reported data were obtained are given in Figs. 2 and 3. In the following paragraphs, we consider all performance data that was obtained at background pressures of less than 1 mTorr. However, it should be noted that:

- There is some question remaining as to the validity of performance measurements taken in the 0.1-1 mTorr pressure range.
- In no cases were the pressure gauge readings corrected for the type of gas (usually some mixture of the propellant used and air) being measured. In general, the gauges were calibrated for nitrogen (air).
- The lithium data was generally taken at background pressures an order of magnitude or more lower than the lowest reported gas-fed P_b.
- The effects of ambient lithium vapor pressure in the vicinity of the thruster (which would not be measured by the vacuum pressure gauges) is not considered in any of the results presented.
- Although the performance data taken at background pressures above 1 mTorr may not provide valid absolute performance measurement which can be compare with other data, this data is still of much value. As long as the background pressure remains constant over the series of experiments, observed performance trends should be valid and can provide insight into AF-MPDT optimization and scaling.

5 Some Non-Dimensional Performance Parameters

We now define several non-dimensional parameters to aid in comparing the different thruster designs across different propellants, mass flow rates, powers levels, and applied field strengths. One obvious parameter which we will use and which commonly appears in MPDT literature is the ratio of the anode to cathode radius; $\bar{R} \equiv R_a/R_c$.

We also expect the ratio of the applied magnetic field strength to the self induced one to be an important parameter in determining the relative importance of self-field to applied-field contributions to thrust and voltage. We will define such a ratio, $\bar{B}$ as:

$$\bar{B} \equiv \frac{B_A}{B_{SF}} = \frac{2\pi R_c B_A}{\mu_o J} \tag{1}$$

Where the applied field (B_A) is measured on the thruster centerline at the cathode tip and the induced field (B_{SF}) is calculated at the cathode outer radius.

For the operation of self-field thrusters, where $\bar{B} = 0$, a critical ionization current has been defined based upon an equal partition of energy between plasma acceleration and ionization processes [18]. The critical

ionization current (J_{ci}), as it is referred to, is defined as:

$$J_{ci} = \sqrt{\frac{4\pi \dot{m} u_{ci}}{\mu_o \ln(\bar{R})}}, \tag{2}$$

where,

$$u_{ci} = \sqrt{\frac{2e\epsilon_i}{M_i}} \tag{3}$$

ϵ_i is the propellant ionization potential and M_i is the ion mass. The ratio of this current to the operating current ($\xi \equiv J/J_{ci}$) has been demonstrated experimentally to scale the performance (thrust and specific impulse) of various thruster designs and operating ranges. It follows that, for thrusters operating in self-field mode, similar thrust and specific impulse can be expected at similar values of ξ. In addition, operation at $\xi > 1$ has been shown to correspond to the appearance of current-driven instabilities and large voltage fluctuations (the onset condition discussed in Sec. 2) which cause a decrease in performance and an increase in erosion. Since self-field thruster performance increases with operating current, the best performance is usually obtained at $\xi \approx 1$. The parameter ξ is then a useful scaling parameter for self-field thrusters:

$$\xi = \frac{J}{J_{ci}} = \sqrt{\frac{\mu_o \ln(\bar{R})}{4\pi u_{ci}}} \frac{J}{\sqrt{\dot{m}}} \tag{4}$$

A second approach to an analytical description of the onset current was developed by Tikhonov [57]. The Tikhonov relation is based upon an estimate of the ratio of electromagnetic to gas dynamic pressure, A_o, at the location of transition from subsonic to supersonic flow ($M = 1$). Tikhonov defines A_o as:

$$A_o = \frac{\mu_o \gamma J^2}{8\pi a_o \dot{m}} \tag{5}$$

Where a_o is the plasma sound speed:

$$a_o = \sqrt{\frac{\gamma k T_e}{M_i}} \tag{6}$$

A critical current, J^*, is defined empirically by plotting A_o versus $\bar{R}$ for data taken from several different thrusters operating at onset. Equating the fit to the general expression for A_o, Tikhonov found:

$$J^* = \sqrt{\frac{28.8\pi a_o \dot{m}}{\mu_o \gamma (\bar{R} - \frac{1}{2})}} \tag{7}$$

The ratio of the operating current to J^* , which we will refer to as ξ_T, performs a similar role as ξ defined earlier:

$$\xi_T \equiv \frac{J}{J^*} = \sqrt{\frac{\mu_o \gamma (\bar{R} - \frac{1}{2})}{28.8\pi a_o}} \frac{J}{\sqrt{\dot{m}}} \tag{8}$$

We will see that over a wide range of operating conditions the values of ξ and ξ_T agree well despite the different theories on which they are based. This was also observed by Choueiri [18].

No such general scaling relation yet exists for the applied-field thruster where $\bar{B} \gg 1$. However, Tikhonov et. al. [57] have developed an empirical relation for applied-field thrusters following the self-field case which predicts the limit of stable operation (onset) well in several thruster designs. The AF A_o is written by Tikhonov as:

$$A_o^B \equiv \frac{(R_a - R_c) J B_A}{4\pi a_o \dot{m}} \tag{9}$$

And, in a similar manner to the self-field case, the critical current (J_B^*) and the ratio of the applied current to the critical current can be written:

$$J_B^* = \frac{14.4\pi a_o \dot{m}}{B_A R_a \left(1 - \frac{1}{\bar{R}}\right)\left(\bar{R} - \frac{1}{2}\right)} \tag{10}$$

$$\xi_B = \frac{J}{J_B^*} = \frac{\left(1 - \frac{1}{\bar{R}}\right)\left(\bar{R} - \frac{1}{2}\right) R_a J B_A}{14.4\pi a_o \dot{m}} \tag{11}$$

As defined, ξ_T and ξ_B are purely statements of the predicted stable operating limit of a given thruster. It is expected that operation above $\xi_T \approx 1$, for self-field thrusters, and $\xi_B \approx 1$, for applied-field thrusters, results in a decrease in performance, voltage fluctuations, and increased erosion. However, they may also prove useful as more general performance scaling parameter in the same way that the critical ionization current (J_{ci}) scales the performance and onset in self-field thrusters. From Eq. 10, we note that the critical current should decrease with increasing B_A. Since thrust and I_{sp} generally increase with B_A, Eq. 10 suggests that an optimal B_A may exist. Such an optimum has been modeled by Tikhonov [57] based upon this relation, and observed empirically by many authors (see [2, 42] for example).

We also note that ξ_B (Equation 11) is proportional to $R_a J B_A / \dot{m}$. A similar scaling for specific impulse (I_{sp}) in the applied field thruster has been proposed and observed by several groups ([3, 13], and others). We therefore expect that higher I_{sp}'s will require higher ξ_B operation.

Thruster	Group	References
MAARC	AVCO-Everett	[20, 21, 22]
X-2C	AVCO-RAD	[23, 24, 25, 26, 27]
X-2-Alkali	AVCO-RAD	[23, 28]
LAJ-AF-CG	Electro-Optical Systems	[29, 30, 31]
LAJ-AF-2	EOS/Lewis	[32, 33]
HC-8	Los Alamos	[5] [4, 3]
MAI-30kW	Moscow Aviation Institute	[13, 34]
MAI-150kW	Moscow Aviation Institute	[35, 36, 34, 37, 38]
MAI-200kW	Moscow Aviation Institute	[39, 40, 13]
MY-III	Osaka University	[41, 42, 43, 44, 45, 46]
Myers100kW	Sverdrup/ Lewis	[47, 48, 49, 50]
Tokyo10-kW	Tokyo U.	[51, 52, 53]
X9	Stuttgart/ DFVLR	[54, 55]
X16	Stuttgart/DFVLR	[54]

Table 1: List of References for Previous Experimental AF-MPDT Work

Thruster	T_e (eV)	Note and Reference
MAARC	2.0	estimate; not much data
X-2C	2.0	1 eV measured 17 cm downstream [25]
X-2-Alkali	2.0	estimate; no data
LAJ-AF-CG	2.0	estimate; no data
LAJ-AF-2	2.0	estimate; no data
HC-8	1.0	[4]
MAI	2.0	[37] [35]
Myers100kW	1.7	[49]
Tokyo10kW	2.0	[51]
X9	2.0	measured to be between 2.6-0.86 [55]
X16	2.0	no data
MY-III	5.0	varies with B_A from 4-6 eV [42]

Table 2: Electron Temperatures Used for ξ_T and ξ_B Calculations with References

The evaluation of ξ_B and ξ_T require that the electron temperature (T_e) be known. For the literature reviewed, this data was not always available. When it was, the details of the measurement method and measurement location were not always clear. In some cases, different values (by a factor of 2) were reported for the same thruster and operating conditions in different references. In Table 2, we summarize the values of T_e that were used for our calculations of ξ_T and ξ_B. Where data were available the reference is noted. Where no data were found, we estimate that T_e was close to the measurements of similar thrusters and take it to be 2 eV.

We are now able to calculate each of the non-dimensional parameters defined in this section ($\bar{B}$, ξ, ξ_T and ξ_B) for the thrusters presented in Fig. 1. For our calculations, we use the operating and performance values from Figs. 2 and 3 with the T_e values from Table 2. The results are presented in Fig. 6 for the gas-fed thrusters and in Fig. 7 for the alkali vapor thrusters. It is apparent that our parameter space is large; $\bar{B}$ varies from 0.08 for the high-power quasi-steady MY-III thruster to 300 for the Stuttgart X16 design and ξ_B can be as high as 15 in AVCO-RAD's X-2-Alkali thruster and as low as 0.006 for the MY-III.

6 Summary of Performance

In discussing the performance of AF-MPDTs we necessarily neglect that data with reported background pressures greater than 10^{-3} Torr. As discussed earlier (Section 4), there is some question about the effects of ambient gases on thruster performance at pressures between 10^{-4} and 10^{-3} Torr. We note that the gas-fed data taken at NASA-Lewis by Myers and Mantenieks and at the University of Tokyo (Arakawa, Kimura and Sasoh) fall into this pressure regime. In fact, the only AF-MPDT data reviewed that were taken at pressures below 10^{-4} Torr was with the condensable alkali metal propellants or the quasi-steady MY-III thruster. For completeness, we note that there is mention in the literature of low pressure gas-fed data (hydrogen and ammonia) taken with the AVCO-RAD X-2C thruster[27] and the McDonnell Douglas Corp. MDX-4A and MDX-7 thrusters [63] in the low-pressure Lewis vacuum facilities. Unfortunately, the data plots are unavailable at this time.

In Table 8, we list typical operating points for each thruster meeting our criteria of $P_b \leq 10^{-3}$ Torr. Operating conditions (J, B_A, $\dot{m}$, propellant, $\bar{R}$), and performance measurements (power, η, I_{sp}, and T/P) are given, listed in order of decreasing efficiency. Power to the applied magnetic field and power to vaporize condensable propellants are neglected. Also included are the calculated non-dimensional parameters ($\bar{B}$, ξ, ξ_T and ξ_B) discussed in Section 5. The references from which the data were taken are listed in Table 3. In all cases, the best performance points (η and I_{sp}) available for each thruster design and propellant are given. In addition, for thrusters operating over a wide range of applied fields, currents, and/or mass flow rates, typical performance at other $\bar{B}$, ξ_T, and ξ_B conditions are provided. In the case of the EOS LAJ-AF-2 thruster data taken at NASA-Lewis, we lacked enough data to compute all the performance parameters. This thruster is included in Figure 8 with estimates made from what data was available.

Three distinct power regimes can be identified in the available data. Most of the alkali metal data, with the exception of the MAI work, was obtained at low powers (< 30 kW). The gas-fed thruster work at Tokyo University also falls into this category. At moderate powers (30-200 kW) we have data from Myers' 100kW argon thruster and the MAI lithium thrusters. At high power (> 200 kW) published experience with applied-fields is limited to the quasi-steady data taken by Tahara at Osaka University. We now examine the η versus I_{sp} and Thrust versus JB_A curves in each of these regimes. We choose T versus JB_A for our comparison because it has been observed by many authors that the thrust in AF-MPDTs is proportional to the product of the current and the applied field. The anode radius also appears to play a fundamental role in the scaling, with a linear, $T \propto JBR_a$, [3] [35] or a quadratic, $T \propto JBR_a^2$, scaling [47] proposed.

Examining the low power data (Figs. 9 and 10), we have the results of EOS and NASA-Lewis at lithium flow rates of 7-14 mg/s and powers less than 30 kW, The 30-kW MAI data with lithium at flow rate of 14-20 mg/s, AVCO-RAD lithium X-2 data at 1-7 mg/s and 4-7 kW, and Tokyo University with argon, helium, and hydrogen flow rates of 9, 2, and 1 mg/s, respectively at under 10 kW of power.

In Fig. 9, we note that η increases with I_{sp} for all the low power thrusters reviewed. There is good agreement between the data taken at EOS and that at NASA-Lewis using a similar thruster. The MAI thruster performance at similar powers and mass flow

Thruster	Group	Propellant	Current (A)	R_a/R_c	B_A/B_{sf}	ξ	ξ_T	ξ_B
MAARC	AVCO-Everett	H_2, NH_3, N_2, Ar	300-1600	1.99	< 8.3	0.1-0.3	0.14-0.34	0.02-0.1
X-2C	AVO-RAD	H_2	300-1600	3.59	4-7.5	0.1-0.34	0.14-0.5	0.07-0.44
MY-III	Osaka U.	H_2, N_2-$2H_2$, Ar	3000-18000	**6.04**	**0.15-2.8**	**0.4-1.4**	**0.5-1.7**	**0.1-2.3**
MY-III	Osaka U.	H_2, NH_3	3000-18000	**6.04**	**0.08-1.2**	**0.1-0.5**	**0.1-0.6**	**0.006-0.13**
X16	Stuttgart	Ar, Xe, Kr	50-100	5.00	225-300	0.1-0.2	0.16-0.22	5.7-8.2
X9	Stuttgart	Ar, He	400-1200	4.00	1.5-8	0.2-0.44	0.3-0.6	0-0.7
AF100kW-A	Sverdrup/Lewis	H_2	750	**3.91**	**1.5-3.6**	**0.24**	**0.34**	**0.09-0.23**
AF100kW-A (B,C)	Sverdrup/Lewis	Ar	750-2000	**3.91 (5.95, 7.97)**	**0.7-8.5**	**0.3-0.6**	**0.4-0.8**	**0.1-1.0**
AF100kW-G	Sverdrup/Lewis	Ar	1000	**5.95**	**2.5-5**	**0.45**	**0.7**	**1.2-2.2**

Figure 6: Gas-Fed Thrusters: Non-Dimensional Parameter Ranges Computed from Performance Parameters in Fig. 2. $P_b < 1$ mTorr shown in **bold.**

Thruster	Group	R_a/R_c	B_A/B_{SF}	ξ	ξ_T	ξ_B
X-2-Alkali	AVCO-RAD	6.97	10-29	0.25-0.35	0.3-0.4	1-15
LAJ-AF-CG	EOS	2.98	10-24	0.2-0.3	0.2-0.3	0.3-0.6
HC-8	Los Alamos	1.98	17-44	~0.14	~0.16	0.08-.2
MAI-30kW	MAI	2.92	6-15	0.3-0.6	0.4-0.7	0.5-1.0
MAI-150kW	MAI	3.56	2-8	0.5-0.8	0.5-0.9	0.5-1.5
MAI-200kW	MAI	3.04	2-4	0.7-0.9	0.7-0.9	0.5-1.3
EOS LAJ-AF-2	EOS/NASA-Lewis	3.00	5-30	0.2-0.5	0.2-0.5	0.2-1.0

Figure 7: Alkali Vapor Thrusters: Non-Dimensional Parameter Ranges Computed from Performance Parameters in Fig. 3. All P_B's were less than 1 mTorr.

thruster	propellant	R_a/R_c	Current (A)	Power (kW)	B_A (T)	Mass Flow Rate(mg/s)	T/P (mN/kW)	**η (%)**	I_{sp} (s)	B_{AF}/B_{SF}	ξ	ξ_T	ξ_B
LAJ-AF-2 (Lewis)	lithium	2.98		20.78		10.0	25.8	**69**	5468				
LAJ-AF-2 (Lewis)	lithium	2.98		17.29		10.0	25.7	**57**	4527				
LAJ-AF-CG-1C	lithium	2.98	280	20.30	0.26	11.4	24.7	**55**	4491	23.04	0.25	0.24	0.52
LAJ-AF-2 (Lewis)	lithium	2.98		20.49		10.0	22.3	**51**	4663				
LAJ-AF-CG-1C	lithium	2.98	282	22.14	0.26	11.4	22.9	**51**	4535	22.87	0.25	0.24	0.52
MAI200kW	lithium	3.04	2900	185.54	0.09	107.0	24.0	**50**	4240	4.08	0.85	0.83	1.08
LAJ-AF-CG-1C	lithium	2.98	300	18.00	0.15	11.4	24.6	**48**	3965	12.54	0.27	0.26	0.32
MAI150kW	lithium	3.56	2100	121.80	0.09	94.0	27.0	**47**	3568	4.82	0.70	0.70	1.15
MY-III	hydrogen	6.04	15412	3629.63	0.20	400.0	10.2	**47**	9415	0.31	1.39	1.72	0.88
MY-III	hydrogen	6.04	14520	3102.92	0.30	400.0	11.0	**47**	8694	0.50	1.31	1.62	1.24
MY-III	hydrogen	6.04	15412	3391.02	0.10	400.0	10.4	**46**	8987	0.16	1.39	1.72	0.44
MAI150kW	lithium	3.56	2000	122.04	0.09	81.0	24.2	**44**	3724	5.06	0.72	0.72	1.27
MY-III	hydrogen	6.04	14141	3357.20	0.05	2750.0	26.6	**43**	3316	0.08	0.49	0.60	0.03
MAI30kW	lithium	2.92	800	32.89	0.10	20.0	22.5	**42**	3769	7.50	0.53	0.51	0.72
MAI30kW	lithium	2.92	900	38.64	0.10	20.0	20.7	**41**	4077	6.67	0.60	0.58	0.81
MY-III	hydrogen	6.04	14285	3236.03	0.40	400.0	9.9	**39**	8135	0.67	1.29	1.59	1.63
MY-III	hydrogen	6.04	15751	3875.30	0.50	400.0	8.8	**38**	8694	0.76	1.42	1.75	2.25
MAI150kW	lithium	3.56	1800	80.13	0.05	86.0	28.0	**37**	2663	2.81	0.63	0.63	0.54
X-2-Alkali	lithium	6.97	150	4.50	0.23	0.9	12.0	**36**	6111	24.23	0.63	0.74	15.23
MAI200kW	lithium	3.04	2800	122.93	0.05	92.0	23.0	**35**	3127	2.11	0.88	0.86	0.61
HC-8	lithium	1.98	407	20.00	0.27	35.0	35.0	**35**	2050	31.51	0.16	0.15	0.14
MAI150kW	lithium	3.56	1800	97.44	0.05	51.0	18.6	**33**	3621	2.81	0.81	0.82	0.91
Myers100kW	argon	3.91	1000	59.45	0.17	100.0	28.8	**25**	1747	5.29	0.40	0.55	0.89
Myers100kW-G	argon	3.91	1000	115.37	0.15	100.0	19.9	**23**	2337	4.80	0.45	0.70	2.20
Tokyo10kW	argon	5.50	85	3.06	0.25	9.0	36.6	**23**	1269	58.82	0.13	0.18	1.66
Tokyo10kW	helium	5.50	200	7.00	0.08	1.8	10.6	**22**	4191	7.50	0.33	0.54	1.86
X-2-Alkali	lithium	6.97	150	4.65	0.10	1.8	12.9	**21**	3389	10.66	0.45	0.53	3.35
MY-III	ammonia	6.04	12808	1762.35	0.18	4470.0	32.8	**21**	1318	0.34	0.49	0.63	0.13
Myers100kW	argon	3.91	1500	82.93	0.13	100.0	22.3	**21**	1887	2.77	0.59	0.83	1.05
Tokyo10kW	argon	5.50	110	4.18	0.25	9.0	29.4	**20**	1393	45.45	0.16	0.24	2.15
Tokyo10kW	hydrogen	5.50	200	7.20	0.10	0.9	6.9	**19**	5663	10.00	0.37	0.56	2.69
Myers100kW	argon	7.97	1000	92.12	0.08	140.0	24.1	**19**	1617	2.44	0.41	0.69	1.54
Myers100kW	argon	5.95	1000	88.34	0.12	100.0	20.3	**18**	1829	3.73	0.45	0.70	1.71
Myers100kW	argon	5.95	1250	94.16	0.10	100.0	19.5	**18**	1872	2.53	0.57	0.87	1.81
Myers100kW	argon	7.97	1000	96.00	0.06	100.0	18.4	**16**	1798	2.04	0.49	0.82	1.80
MY-III	hydrogen	6.04	4304	597.00	0.30	400.0	13.0	**13**	1976	1.67	0.39	0.48	0.37
Tokyo10kW	hydrogen	5.50	200	7.80	0.08	0.9	5.4	**13**	4757	7.50	0.37	0.56	2.02
MY-III	hydrogen	6.04	4304	750.10	0.50	400.0	11.3	**12**	2155	2.79	0.39	0.48	0.61
X-2-Alkali	lithium	6.97	200	7.00	0.14	6.7	11.6	**7**	1239	10.91	0.31	0.36	1.64
Tokyo10kW	nitrogen	5.50	200	6.40	0.25	8.4	11.1	**5**	862	25.00	0.22	0.36	2.70

Figure 8: Typical (Best) Performance Points of the Reviewed Thrusters in Order of Decreasing η

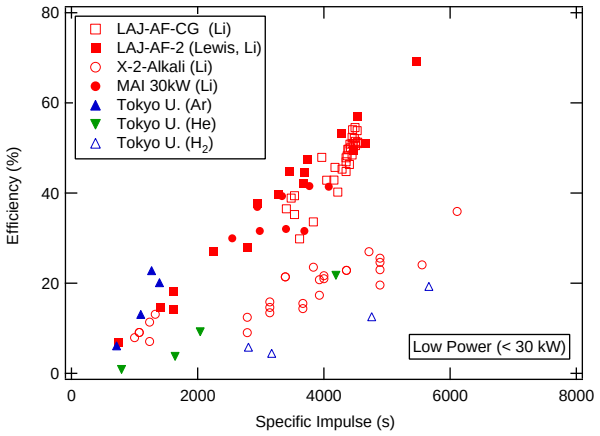

Figure 9: Efficiency versus I_{sp} for Thruster Power < 30 kW

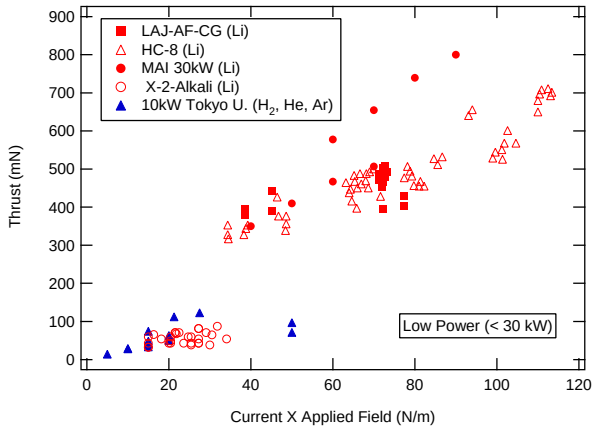

Figure 10: Thrust versus JB_A for Thruster Power < 30 kW

rates also agrees well with the EOS data. The absolute magnitude of the efficiency for a given I_{sp} is greater for the EOS and MAI designs and the Tokyo argon thruster at these powers and mass flow rates. The data with the highest η at a given I_{sp} were taken with the higher power, higher $\dot{m}$ thrusters having $\bar{R} \approx 3$. The lower performing Tokyo University and ACVO-RAD thrusters had $\bar{R}$'s nearly twice the other thrusters and operated at slightly lower $\dot{m}$ and powers of less than 10 kW.

From the T versus JB_A plot (Fig. 10) we see that thrust increases with the product of current and applied magnetic field as excepted. The thrusters are grouped by power level, with the thrusters operating at the highest power and mass flow rates (MAI 30kW and HC-8) demonstrating the largest thrust at the highest JB_A.

In the moderate power range (30-200 kW), we compare the data of Myers 100-kW argon thruster and the Moscow Aviation Institute's lithium thrusters. Both thrusters operated at similar values of $\bar{B}$ and ξ_B. From Fig. 11 we see that the MAI thrusters outperform Myers' AF100kW in both η and I_{sp}. It seems clear that the benefit of the MAI thruster (due to propellant, design, or a combination of both) is its ability to operate at higher I_{sp}'s for a given discharge power. From Myers' 100kW data, performance seems to increase slightly with decreasing $\bar{R}$. However, propellant type and I_{sp} appear to have a greater effect than $\bar{R}$ on efficiency in this power regime. Examining the thrust vs JB_A plot of the same data, we again find the linear scaling we expect. The slope of the thrust vs JB_A curves appear to depend upon geometry ($\bar{R}$) and power level.

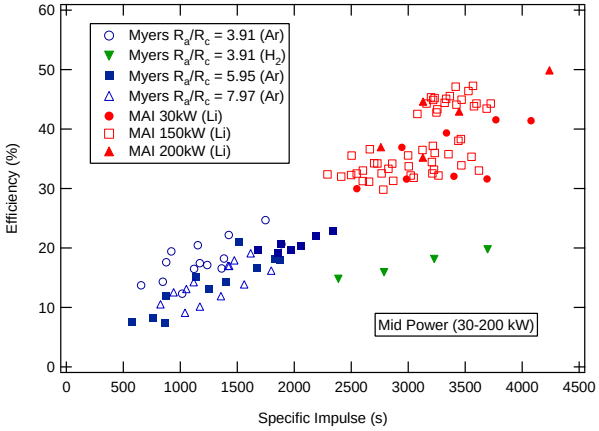

Figure 11: Efficiency versus I_{sp} for Thruster Power $30 - 200$ kW

In the high power range (> 200kW) we are limited to the 200 kW data taken at MAI and the high power (3-18 MW) data from Osaka University. Clearly, the upper end of this regime is the domain of the self-field MPDT. As such, not much work has been done using applied fields.

Values of $\bar{B}$ for the MY-III are low ranging from 0.1 to 2.3 at 400 mg/s of hydrogen, but only increasing over 1 when strong (0.4-0.5 T) fields are applied to the lower current boundary of the MY-III operating regime. Recall that at the low and moderate powers we saw a fairly strong linear scaling of the thrust with JB_A. We illustrate this by plotting the thrust data for two thrusters (the HC-8 and the AF100kW) versus JB_A in Fig. 13. The HC-8 data were taken with

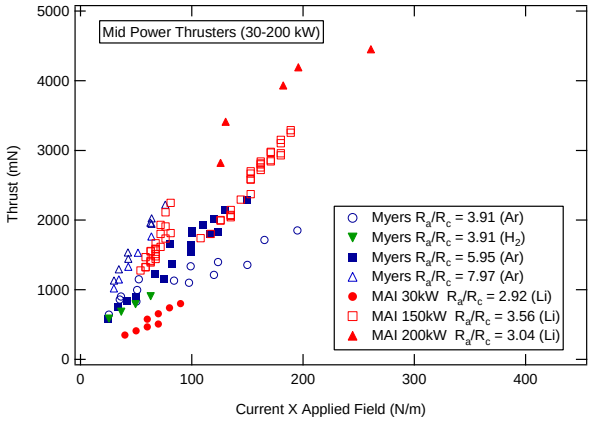

Figure 12: Thrust versus JB_A for Thruster Power $30 - 200$ kW

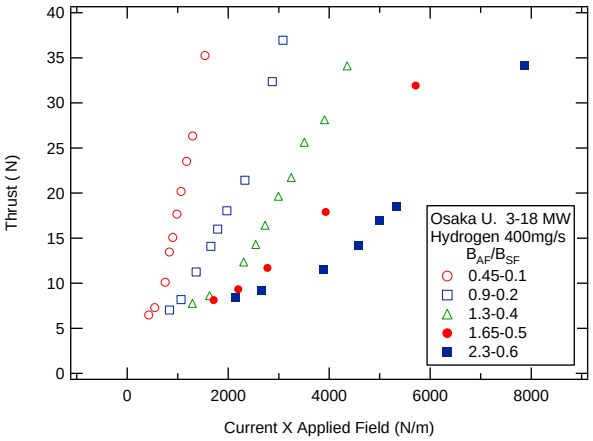

Figure 14: Scaling of the High Power, Low $\bar{B}$ MY-III Thruster with JB_A

lithium at 20 kW with $\bar{B} \approx 17 - 44$. The AF100kW data was taken with argon at $\bar{B} \approx 3 - 5$. We contrast this data with Fig. 14 which shows the same curve for the MY-III thruster at powers of 3-18 MW and a single propellant and flow rate. Clearly JB_A is not the proper scaling at the higher powers examined. Although we do see that, at the highest applied field values, $\bar{B}$ does increase above one at the lower currents and the curves begin to collapse to a single line.

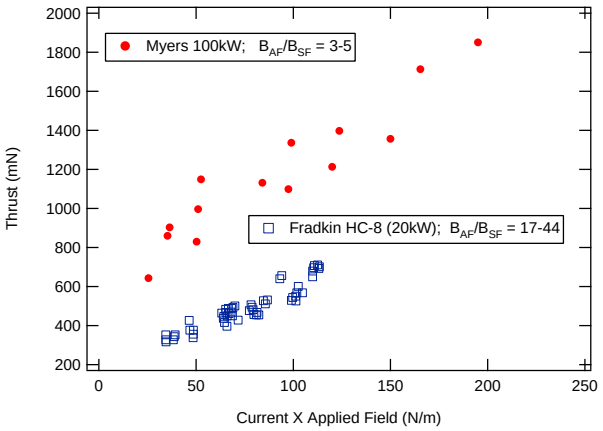

Figure 13: Scaling of Two High $\bar{B}$ Thrusters with JB_A

Plotting η versus I_{sp} for the high power thrusters (Fig. 15), we immediately note the high efficiency and I_{sp} of the MAI thruster operating at one-half to one-quarter the power of the MY-III thruster. Efficiency increases linearly with I_{sp} and is higher for higher $\dot{m}$ at a constant I_{sp}. As expected, the scaling of thrust with JB_A is not good and there is a large spread in the slopes of T vs IB_A curves for a single thruster design (MY-III).

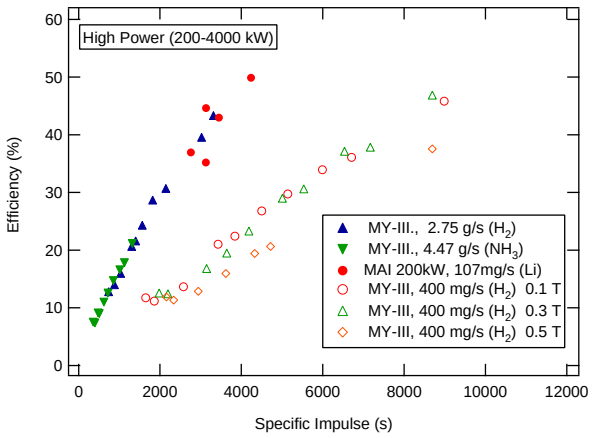

Figure 15: Efficiency versus I_{sp} for Thruster Power 200 kW to 4 MW

Finally, we examine how well Tikhonov's non-dimensional parameter ξ_B scales the data we've presented here. As ξ_B takes into account all of our controllable parameters, J, B_A, $\dot{m}$, propellant (through a_o), and geometry (through R_a and $\bar{R}$) we expect, if it is a valid scaling parameter for AF-MPDTs, for it to collapse all of the data, regardless of thruster, propellant, or power level, to a single line.

We find that ξ_B is a reasonable scaling parameter for thrusters operating at moderate powers ($\sim$ 30-150 kW) and at moderate flow rates ($\sim$ 10-100 mg/s).

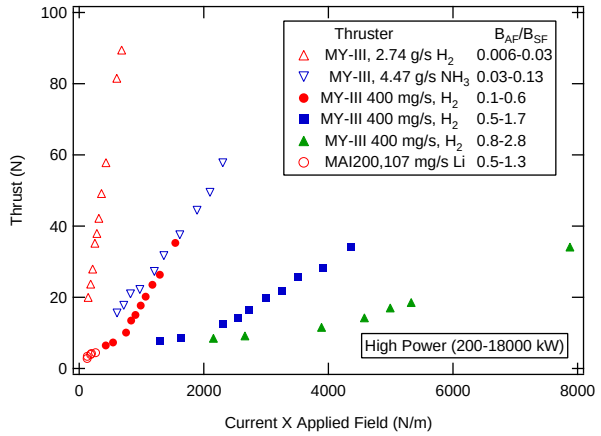

Figure 16: Thrust versus JB_A for Thruster Power 200 kW to 4 MW

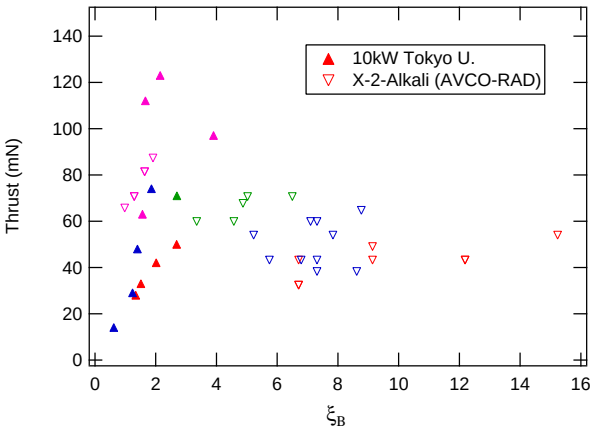

Figure 18: Thrust Scaling withξ_B at high ξ_B

We plot thrust versus ξ_B for these thrusters in Fig. 17. Thrust increases linearly with ξ_B and the increase appears to be more rapid at the lowest ξ_B's for $\xi_B \lesssim 2$. The data from various thrusters and propellants collapse somewhat to a single line, although there is still enough scatter to suggest that the definitive scaling parameter has not yet been found. At constant thruster power, the data scatter increases with increasing mass flow rate. An increase or decrease in power also appears to increasing the scatter.

For the low power thrusters (AVCO-RAD X-2 and

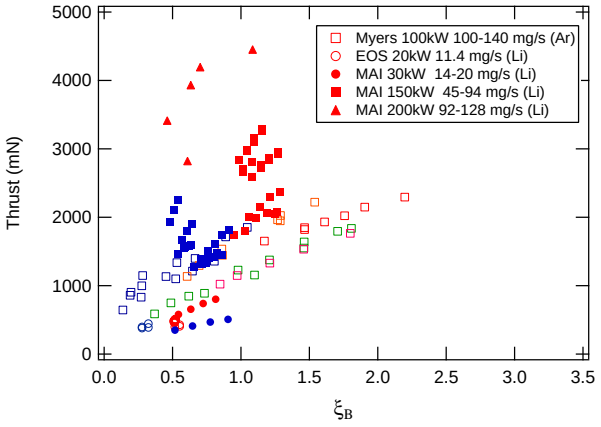

Figure 17: Scaling of Thrust with ξ_B

Tokyo U. 10kW) no strong correlation was found with ξ_B. The thrust appears to change from an increasing function of ξ_B to a decreasing function of ξ_B at a ξ_B value of about 4-5 (Fig. 18). However, our data in the $\xi_B > 4$ range is limited to a single thruster in a limited $\dot{m}$ and power range, and this trend needs to be validated with additional data. For the high power data ξ_B was generally less than 1 and thrust increased rapidly with increasing ξ_B. However, the scatter was large, even for a single thruster design and mass flow rate and no scaling with ξ_B was found.

7 Design Theory and Optimization

In this section we take a more detailed look at the conclusions of each group with respect to several thruster design considerations; Geometry and Electrode Design, Applied Field Shape, Current Outflow, and Propellant and Propellant Injection. Our current scaling parameter, ξ_B, while it has some sensitivity to propellant (through a_o) and geometry (through $\bar{R}$), does not take into account these differences between thrusters. We will see in the following paragraphs however, that they can have a significant effect on AF-MPDT performance.

7.1 Electrode Design and Geometry

The most extensive study of geometry effects in AF-MPDTs has been conducted by Myers [47, 48]. Eight thruster geometries were tested at a constant current of 1000 A and a constant argon flow rate of 100 mg/s. Several groups in Russia have also done detailed empirical and theoretical studies of MPDT geometry. The MAI thruster design is based upon at least a decade of empirical studies, many of which are still

inaccessible but are summarized in MAI technical reports from 1994-1998 [59, 58].

Cathodes recessed within the discharge chamber demonstrate superior performance to those extending to the thruster exit plane or beyond [47, 65]. The structure of the plume was also reported to be significantly different for the shorter cathode [47]. Hollow cathode (HC) operation is superior to solid cathode operation. The hollow cathode thruster exhibits smaller voltage and current fluctuations and less melting at similar operating conditions than the solid rod cathode [4]. Furthermore, a multi-channel hollow cathode (MCHC) design was found empirically to operate with lower erosion rates than solid rod or hollow cathodes [59]. The MCHC also operates better at lower $\dot{m}$ than rod cathodes or hollow cathodes due to greater emitting surface [58]. The highest performance (η, Thrust) at MAI was observed when the tungsten rods making up the multi-channels were recessed 0.3 - 0.75 internal cathode diameters from the cathode exit plane [66].

Profiling the anode to parallel the magnetic field lines resulted in more uniform current density distribution and lower anode temperatures in work in Russia [37]. Tahara and Myers found better results with diverging anodes [65, 50]. A hot, radiating anode (as opposed to a water-cooled design) was also found to improve current transfer and to reduce losses [10]. Although, a study by AVCO-RAD [67] comparing the operation of a radiation-cooled and a water-cooled X-7 thruster operating on ammonia at 400-600 A found no difference in overall performance. While the water-cooled version operated at higher voltages, the thrust was also generally higher, rendering the performance differences negligible.

The fundamental effect of anode and cathode radii on AF-MPDT performance has been demonstrated by several authors [47, 34, 68, 69, 65]. Thrust and voltage are generally observed to increase linearly or quadratically with R_a. From theoretical models, the group at MAI showed that reducing the anode-cathode ratio ($\bar{R}$) resulted in stable operation at higher discharge currents (i.e. increased J^*) [34]. Empirically, MAI found the current density limit for low erosion operation with a multichannel hollow cathode to be $j_c \leq 200$ A/cm^2 [36]. The widest stable operating range was found by semi-empirical models, again for the MCHC and profiled anode, to correspond to $\bar{R} = 3{-}3.5$ [68], [69]. This result is similar to that reported in [11]. Myers measured the maximum efficiency with his smallest radius anode ($\bar{R} = 3.9$) and determined that it was due to a larger fraction of plasma power being converted into thrust power as R_a was reduced. However, the slope of the efficiency versus I_{sp} curve decreased with decreasing anode radius and higher magnetic fields were required to reach the same I_{sp} as $\bar{R}$ decreased. This implies that an optimum $\bar{R}$ for a given operating regime should exist, similar to what was found in the MAI studies.

7.2 Applied Magnetic Field Shape

Several groups have investigated the effects of applied field strength and shape on performance. In general, η, I_{sp} (or T) and V_d increased linearly with applied-field strength for $\bar{B} \gg 1$ [35, 47, 55, 20]. At powers less than 100 kW, operation without an applied field usually resulted in a diffuse beam. The addition of an applied field produced the characteristic cathode and anode jets which extended downstream of the anode[35, 4]. Myers observed (100 kW, cylindrical anode, $\bar{B} = 1 - 9$) that, as B_A was increased, a larger fraction of the input power was deposited in the plasma (rather than the electrodes) and was therefore available for conversion to thrust power [47].

Several studies point to the existence of an optimal magnetic field shape and strength[35, 49, 20, 42]. Axial magnetic fields which diverge slowly downstream of the cathode tip have demonstrated the best performance for all $\bar{B}$ values [30, 58, 5, 55, 54]. It was found that reversing (or reducing to close to zero) the magnetic field gradient near the cathode tip degrades performance [30, 34]. The optimum B_A strength appears to be dependent on propellant, flow rate and more weakly on current[42] and to became less pronounced as the field is made more axial in the discharge chamber[20].

For operation near $B_A \approx B_{SF}$, Tahara concludes that the applied field should be kept slightly lower that the self-field at the cathode tip and much less than the self field elsewhere. The best performance was with the applied field shaped to be parallel to the inner anode surface[41, 44], similar to the MAI design philosophy [58]. In contrast to results where $B_A \gg B_{SF}$, discharge current flowed more upstream and a more uniform radial pressure distribution were reported with the application and increase of the applied field. The measured thrust and the critical current were at all points higher for operation with an applied field than with the self-field alone. All performance parameters, V, T, and η, increased with applied field for currents less than 10 kA [65] . The

applied-field had little effect on performance at higher currents, however, it did increased the stable, low-erosion operation region to higher currents (higher I_{sp}'s). This result is in contrast to results reported by MAI at 200 kW. MAI found a decrease in the critical current (smaller operating range) at $\bar{B} = 2$–4. They attributed the decrease to the augmentation of the hall pinching ($j_\theta B_z$) by a self-field pinching ($j_z B_\theta$)[39] leading to anode starvation at lower currents [39].

7.3 Current Outflow

One of the characteristics of the AF-MPDT is the extension of a significant fraction of the current downstream of the thruster geometry [29, 35, 4]. From Section 4 we recall that the plume shape and extent are dependent on background pressure. Current outflow extends the acceleration volume into regions of lower density making the thrust and voltage more sensitive to the ambient environment. Therefore, we only sight evidence of outflow when the background pressure was less than 1 mTorr.

At MAI, the outflow length was defined as the distance from the cathode tip in which 90% of the total current is contained [35]. It was observed that the current outflow was less when the anode was profiled (rather than cylindrical) and decreased by a factor of ten when a hollow cathode was used in place of a solid rod cathode (this also decreased the discharge voltage) [59]. The magnitude of the outflow, for a given thruster design, was observed to depend on the current, magnetic field, and operating regime (electrothermal vs electromagnetic acceleration). At a fixed current, the outflow was proportional to $B_A/\dot{m}$ [70]. This scaling was also reported by other groups [4, 61, 11]. Magnetic probe measurements made using the MAI 150 kW thruster showed that the current outflow length was approximately 1.8 - 2 anode diameters ($\approx$ 30 cm) over the range of stable operation. Fradkin (HC-8) found up to 40% of the arc current at an axial distance 90 cm downstream at 350 A and 0.33 T. The outflow current fraction increased with increasing applied field strength with no outflow detected at magnetic fields below 0.12 T. [4]

At high currents (3-18 kA) Tahara observed a large outflow fraction (up to 60% of the total current) only when the applied field was greater than the self field outside of the main discharge region. If the applied field was properly shaped, the current could be made to flow more upstream in the discharge chamber keeping the voltage low and increasing performance via an increase in electrothermal thrust. [46]

7.4 Propellant, Mass Flow Rate, and Propellant Injection

In research conducted in both the United States and the Soviet Union during the 60s and 70s, the best steady-state MPDT performance was obtained with lithium propellant. Lithium provides characteristically low voltages which lead to high efficiencies in the 250-500 kW power range at moderate I_{sp}'s of 3500-4000 s. It seems clear that this is due, in most part, to the low first ionization potential of lithium (5.4 eV) which, combined with a high second ionization potential (75.6 eV), reduces ionization and other frozen flow losses. In experiments with hydrogen and argon at 100 kW, Myers found that hydrogen produced higher efficiencies specific impulses, and voltages, and was stable over a broader range [71]. This trend has been confirmed by the data summarized in this paper. The only fundamental difference between the two propellants observed by Myers was in the power loss mechanisms. For argon at 25 mg/s, the fraction of the input power deposited in the anode was found to increase with B_A. The opposite trend was observed with hydrogen at the same flow rate [71]. At higher argon flow rates (100 mg/s) the anode power fraction decreased with increasing B_A similar to the hydrogen data at one-fourth the flow rate [47].

At EOS and DFVLR-Stuttgart, performance was improved by feeding all or some of the propellant through the anode [29, 10]. Anode propellant injection was found to ensure good current transfer without instabilities by introducing ions into the region of highest potential drop, allowing them to gain maximum energy from the electric field [10]. Anode losses in the X16 were reduced as the mass flow rate to the anode increased. Thrust was a function mainly of the mass flow rate through the cathode, while voltage depended on the anode flow rate [10].

At low lithium flow rates (5-20 mg/s) and with propellant fed through the anode, the group at EOS found the pressure at the cathode tip to be low ($<$ 10 Torr) and the arc attachment to be diffuse or unstable (alternating between a diffuse and a spot mode) with rather high cathode voltage drops (6-7 V) [33] . A gas-buffered cathode was designed with separate hydrogen, nitrogen, or lithium injection around the cathode. This had the desired effect of increasing the cathode pressure ($\approx$ 50 Torr) and reducing the

power lost to the cathode ($P_c < 1$ V). The cathode attachment was at the tip, the discharge was more stable, and erosion was reduced [29]. The best results at EOS were obtained with lithium propellant fed at the anode and a hydrogen buffer gas around the cathode.

8 Conclusions

In this work, we have reviewed much of the existing experimental performance data for magnetoplasmadynamic thrusters operating with applied magnetic fields (AF-MPDTs). The majority of the data has been obtained at power levels below 30 kW. Much of the performance data obtained with gaseous propellants was obtained at questionable facility background pressures ($P_b > 1$ mTorr). As a result, most of the performance data reviewed in this work was obtained with low-power lithium-vapor thrusters. Low power hydrogen, helium, and argon data from the University of Tokyo and argon and hydrogen data at 100 kW (AF100kW) taken at background pressures of $10^{-3} - 10^{-4}$ Torr were also included. Only two thruster designs were operated in the 100-250 kW power range for which performance data was obtained, the 100 kW thruster (Myers) and the MAI 150kW and 200kW lithium thrusters. The only AF data obtained at powers above 250 kW was taken with the quasi-steady MW-class (Osaka University) thruster operating above 500 kW. Clearly there is a gap in AF-MPDT knowledge in the 250-500 kW power range. Lithium thrusters have demonstrated the best performance to date; 69% at 5500 s with the 20 kW EOS LAJ-AF-2 thruster in the low pressure NASA-Lewis facility. Similar performance (55% at 4500 s) was obtained at EOS with a similar thruster and at MAI (50% at 4240 s), also with lithium, but at higher powers.

The thruster designs and operating regimes were found to span a large parameter space. A non-dimensional scaling parameter (ξ_B) based upon Tikhonov's critical current (J_B^*) was presented to assist in the interpretation of the data. This parameter showed some promise in scaling thrust at modest powers (30-100 kW) and mass flow rates (10-100 mg/s). Thrust was found to increase linearly with increasing ξ_B at $\xi_B \lesssim 2$. The slope of the thrust vs ξ_B curve increased as ξ_B decreases. As a performance scaling parameter ξ_B is lacking in several respects as is seen by the relatively large scatter in the data at different operating regimes and thruster designs. Some additional parameters which are not included in J_B^* but have been found to influence AF-MPDT behavior are; magnetic field shape, current distribution (outflow), propellant injection location, and electrode design.

References

[1] A.C. Ducati, G.M. Giannini, and E. Muehlberger. Experimental results in high-specific impulse thermo-ionic acceleration. *AIAA Journal*, 2:1452–1454, August 1964.

[2] N. M. Nerheim and A. J. Kelly. A critical review of the magnetoplasmadynamic (MPD) thruster for space applications. Number AIAA Paper 67-688, 1967. Sept.

[3] D.B. Fradkin. *Analysis of Acceleration Mechanisms and Preformance of an Applied Field MPD Arc Jet*. PhD thesis, Princeton University, 1973.

[4] D.B. Fradkin, A.W. Blackstock, D.J. Roehling, T.F. Stratton, M. Williams, and K.W. Liewer. Experiments using a 25-kW hollow cathode lithium vapor (mpd) arcjet. *AIAA Journal*, 8(5):886, May 1970.

[5] D.B. Fradkin and D.J. Roehling. Thrust stand performance of a lithium fueled applied field MPD arcjet. In *13th Symposium on the Engineering Aspects of Magnetohydrodynamics*, number VI.11.1 - 5, Stanford University, 1973. March 26-28.

[6] D.W. Esker, J.C. Kroutil, and R.J. Checkley. Radiation cooled MPD arc thruster. Technical Report Contract NAS3-11518, McDonnell Douglas Corporation, St. Louis, Missouri, July 1969.

[7] D.W. Esker, J.C. Kroutil, and R.J. Checkley. Design and performance of radiation-cooled MPD arc thrustors. In *AIAA 7^{th} Electric Propulsion Conference*, number AIAA 69-245, Williamsburg, VA, USA, 1969. March 3-5.

[8] A.W. Blackstock, D.B. Fradkin, D.J. Roehling, and T.F. Stratton. A cesium MHD arc jet. *Journal of Applied Physics*, 39(7):3201–3209, June 1968.

[9] G. Krülle, M. Auweter-Kurtz, and A. Sasoh. Technology and application aspects of applied field magnetoplasmadynamic propulsion. *Journal of Propulsion and Power*, 14:754–762, October 1998.

[10] G. Krülle and E. Zeyfang. Preliminary conclusions of continuous applied field electromagnetic thruster research at dfvlr. In *AIAA 11th Electric Propulsion Conference*, number AIAA-75-417, New Orleans, LA, USA, 1975. March 19-21.

[11] J.E. Sovey and M.A. Mantenieks. Performance and lifetime assessment of magnetoplasmadynamic arc thruster technoloy. *Journal of Propulsion and Power*, 7:71–83, January 1991.

[12] J.E. Polk and T.J. Pivirotto. Alkali metal propellants for MPD thrusters. In *AIAA/NASA/OAI Conf. on Advanced SEI Technologies*, Cleveland, Ohio, 1991. AIAA-91-3572.

[13] G. Popov, V. Kim, V. Tikhonov, S. Semenikhin, and M. Tibrina. The fourth (final) quarterly report on the milestones (a)(4) and (a)(5)(d) of SoW of contract no 960938 between RIAME MAI and JPLto NASA-JPL. Technical report, RIAME, MAI, Moscow, Russia, December 1998.

[14] V.P. Ageyev and V.G. Ostrovsky. High-current stationary plasma accelerator of high power. In 23^{rd} *International Electric Propulsion Conference*, Seattle, WA, USA, 1993. IEPC-93-117.

[15] Edgar Yazid Choueiri. *Electro-Ion Streaming Instabilities of an Electromagnetically Accelerated Plasma*. PhD thesis, Princeton University, October 1991.

[16] A. Sasoh. Simple formulation of magnetoplasmadynamic acceleration. *Phys. Plasmas*, 1:464–469, March 1994.

[17] Robert G. Jahn. *Physics of Electric Propulsion*. McGraw-Hill Book Company, New York, USA, 1968.

[18] Edgar Choueiri. The scaling of thrust in self-field mpd thrusters. *Journal of Propulsion and Power*, 14:744–753, 1998. September-October.

[19] R. A. Moore, G.L. Cann, P.F. Jacobs, and L. R. Gallagher. High specific impulse thermal arc jet thruster technology. Technical Report Technical Report EOS-5090-IR-2, Electro-Optical Systems, Inc., Pasadena, CA, September 1965.

[20] Richard M. Patrick and Arthur M. Schneiderman. Performance charateristics of a magnetic annular arc. *AIAA Journal*, 4:283–290, February 1966.

[21] Arthur M. Schneiderman and Richard M. Patrick. Optimization of the thermal efficiency of the magnetic annular arc. In *AIAA 3rd Aerospace Sciences Meeting*, number AIAA 66-115, New York, NY, USA, 1966. January 24-26.

[22] William E. Powers and Richard M. Patrick. Magnetic annular arc. *Physics of Fluids*, 5:1196–1206, October 1962.

[23] R.R. John and S. Bennett. Arcjet technology: Final report. Technical Report NAS 3-5900, Avco Corporation, Wilmington, MA, December 1965.

[24] William E. Powers. Measurements of the current density distribution on the exhaust of a MPD arcjet. *AIAA Journal*, 5:545–550, March 1967.

[25] William E. Powers. Measurements of the current density distribution on the exhaust of a MPD arcjet. In *AIAA 3rd Aerospace Sciences Meeting*, number AIAA 66-116, New York, NY, USA, 1966. January 24-26.

[26] A. C. Malliaris and D.R. Libby. Velocities of neutral and ionic species in a MPD flow. In *AIAA 7th Aerospace Sciences Meeting*, number AIAA 69-109, New York, NY, USA, 1969. January 20-22.

[27] S. Bennett, R.R. John, G. Enos, and A. Tuchman. Experimental investigation of the MPD arcjet. In *AIAA 5th Electric Propulsion Conference*, number AIAA 66-239, San Diego, CA, USA, 1966. March 7-9.

[28] S. Bennett, G. Enos, and R. John. Cesium fueled MPD arc jet engine performance. In *AIAA* 2^{nd} *Aerospace Sciences Meeting*, number AIAA 65-296, San Francisco, CA, USA, 1965. July 26-29.

[29] G.L. Cann. High specific impulse thermal arc jet thruster technology: Part ii. performance of hall arc jets with lithium propellant. Technical

Report Technical Report AFAPL-TR-65-48 Part II, Electro-Optical Systems, Inc., Pasadena, CA, January 1967. EOS 5090.

[30] G.L. Cann. High specific impulse thermal arc jet thruster technology: Part iii interim report. Technical Report Technical Report AFAPL-TR-65-48 Part IR-III, Electro-Optical Systems, Inc., Pasadena, CA, February 1967.

[31] G.L. Cann, R.L. Harder, and S.T. Nelson. Experimental performance of the ALPHA thrustor. In *AIAA Electric Propulsion and Plasmadynamics Conference*, number AIAA 67-687, Colorado Springs, Colorado, 1967. September 11–13.

[32] Denis J. Connolly, Ronald J. Sovie, Charles J. Michels, and James A. Burkhart. Low environmental pressure MPD arc tests. *AIAA Journal*, 6:1271–1276, July 1968.

[33] R. A. Moore, G.L. Cann, and L. R. Gallagher. High specific impulse thermal arc jet thruster technology: Part i. performance of hall arc jets with lithium propellant. Technical Report Technical Report AFAPL-TR-65-48 Part I, Electro-Optical Systems, Inc., Pasadena, CA, June 1965.

[34] V. Kim, V. Tikhonov, and S. Semenikhin. Fourth quarterly (final) report to NASA-JPL: 100-150 kw lithium thruster research. Technical Report Contract NASW-4851, RIAME, MAI, Moscow, Russia, April 1997.

[35] V. Kim, V. Tikhonov, and S. Semenikhin. The final report of the contract on the research studies NASW-4851 between RIAME MAI and NASA. Technical report, RIAME, Moscow Aviation Institute, Moscow, Russia, December 1995.

[36] V. Kim, V. Tikhonov, and S. Semenikhin. The second quarterly report on the stages ##2a, b of the contract on the research studies NASW-4851 between RIAME MAI and NASA. Technical report, RIAME, Moscow Aviation Institute, Moscow, Russia, July 1996.

[37] V.B. Tikhonov, S.A. Semenihin, J.R. Brophy, and J.E. Polk. The experimental performance of the 100 kW lithium MPD thruster with external magnetic field. In 24^{th} *International Electric Propulsion Conference*, Moscow, Russia, 1995. IEPC-95-105.

[38] V.B. Tikhonov, S.A. Semenihin, J.R. Brophy, and J.E. Polk. Performance of 130 kw MPD thruster with an external magnetic field and Li as propellant. In 25^{th} *International Electric Propulsion Conference*, Cleveland, Ohio, USA, 1997. IEPC-97-117.

[39] Victor B. Tikhonov, Sergei A. Semenikhin, and James E. Polk. Own magnetic field impact on MPD thrusters performance with external magnetic field. In 26^{th} *International Electric Propulsion Conference*, number 99-176, Kitakyushu, Japan, 1999. October 17-21.

[40] G. Popov, V. Kim, and V. Tikhonov. The first quarterly report on the items 1 and 2 of contract no. 960938 betweenRIAME MAI and JPL (USA) . Technical report, RIAME, MAI, Moscow, Russia, September 1997.

[41] Hirokazu Tahara, Yoichi Kagaya, and Takao Yoshikawa. Performance and acceleration process of quasisteady magnetoplasmadynamic arcjets with applied magnetic fields. *Journal of Propulsion and Power*, 13:651–658, 1997. September–October.

[42] Hirokazu Tahara, Yoichi Kagaya, and Takao Yoshikawa. Effects of applied magnetic fields on performance of a quasisteady magnetoplasmadynamic arcjet. *Journal of Propulsion and Power*, 11:337–342, 1995. March–April.

[43] H. Tahara, M. Sasaki, Y. Kagaya, and T. Yoshikawa. Thruster performance and acceleration mechanisms of a quasi-steady applied-field MPD arcjet. In *AIAA/DGLR/JSASS 21st International Electric Propulsion Conference*, number AIAA 90-2554, Orlando, FL, USA, 1990. July 18–20.

[44] Hirokazu Tahara, Yoichi Kagaya, and Takao Yoshikawa. Quasisteady magnetoplasmadynamic thruster with applied magnetic field for near earth missions. *Journal of Propulsion and Power*, 5:713–717, 1989. November–December.

[45] H. Tahara, H. Yasui, Y. Kagaya, and T. Yoshikawa. Thruster performance and acceleration mechanisms of a quasi-steady applied-field MPD arcjet. In *AIAA/DGLR/JSASS 19th International Electric Propulsion Conference*, number AIAA 87-1001, Colorado Springs, CO, USA, 1987. May 11–13.

[46] H. Tahara, Y. Kagaya, and T. Yoshikawa. Hybrid MPD thruster with axial and cusp magnetic fields. In *20th International Electric Propulsion Conference*, number IEPC 88-058, Garmisch-Partenkirchen, Federal Republic of Germany, 1988. October 3–6.

[47] Roger M. Myers. Geometric scaling of applied-field magnetoplasmadynamic thrusters. *Journal of Propulsion and Power*, 11:343–350, 1995. March-April.

[48] Roger M. Myers. Scaling of a 100-kw class applied-field MPD thruster. In *AIAA/SAE/ASME/ASEE 28th Joint Propulsion Conference and Exhibit*, number AIAA-92-3462, Nashville, TN, USA, 1992. July 6-8.

[49] Roger M. Myers. Applied-field mpd thruster performance with hydrogen and argon propellants. *Journal of Propulsion and Power*, 9:781–784, 1993.

[50] Maris A. Mantenieks, James S. Sovey, Roger M. Myers, Thomas W. Haag, Paul Raitano, and James E. Parkes. Performance of a 100-kw class applied-field MPD thruster. In *AIAA/SAE/ASME/ASEE 25th Joint Propulsion Conference and Exhibit*, number AIAA-89-2710, Monterey, CA, USA, 1989. July 10-12.

[51] A. Sasoh and Y. Arakawa. Electromagnetic effects in an applied-field magnetoplasmadynamic thruster. *Journal of Propulsion and Power*, 8:98–102, 1992. Jan–Feb.

[52] Y. Arakawa and A. Sasoh. Steady-state permanent magnet magnetoplasmadynamic thruster. *Journal of Propulsion and Power*, 5:301–304, 1989. May–June.

[53] I. Kimura and Y. Arakawa. Effect of applied magnetic field on physical processes in an MPD arcjet. *AIAA Journal*, 15:721–724, 1977. May.

[54] G. Krülle and E. Zeyfang. Preliminary conclusions of continuous applied field electromagnetic thruster research at dfvlr. In *AIAA 11th Electric Propulsion Conference*, number AIAA-75-417, New Orleans, LA, USA, 1975. March 19-21.

[55] G. Krülle. Characteristics and local analysis of MPD thruster operation. In *AIAA Electric Propulsion and Plasmadynamics Conference*, number AIAA- 67-672, Colorado Springs, CO, USA, 1967. September 11-13.

[56] Roger M. Myers. Scaling of a 100-kw class applied-field MPD thruster. In *AIAA/SAE/ASME/ASEE 28th Joint Propulsion Conference and Exhibit*, number AIAA-92-3462, Nashville, TN, USA, 1992. July 6-8.

[57] N.V. Belan et al. *Stationary Plasma Thrusters*. Translated from Russian by R. Spektor, 1989 edition.

[58] V. Kim, V. Tikhonov, and S. Semenikhin. The first quarterly report on the stages # 1- 2 of the contract on the research studies NASW-4851 between RIAME MAI and NASA. Technical report, RIAME, Moscow Aviation Institute, Moscow, Russia, September 1994.

[59] G.A. Dyakonov, G.A. Popov, V.B. Tikhonov, V.A. Petrosov, B.A. Arkhipov, and N.A. Maslennikov. Experimental research of high power MPD-thrusters in pulsed, quasis-tationary and stationary modes. In 30^{th} *AIAA/ASME/SAE/ASEE Joint Propulsion Conference*, number 94-2994, Indianapolis, IN, 1994. June 27-29.

[60] A. C. Ducati, Giannini, and E. G. M.Muehlberger. Recent progress in high specific impulse thermo-ionic acceleration. In *AIAA* 2^{nd} *Aerospace Sciences Meeting*, number AIAA 65-69, New York, NY, USA, 1969. January 25-27.

[61] R.J. Sovie and D.J. Connolly. Effects of backgrounds pressure on magnetoplasmadynamic thruster operation. *Journal of Spacecraft and Rockets*, 7:255–258, March 1970.

[62] Robert E. Jones and Eddie L. Walker. Status of large vacuum facility tests of MPD arc thrusters. In *AIAA* 3^{rd} *Aerospace Sciences Meeting*, number AIAA 66-117, New York, New York, 1966. January 24-26.

[63] D.J. Connolly and R.J. Sovie. The effect of background pressure and magnetic field shape on MPD thruster performance. In *AIAA* 7^{th}

Electric Propulsion Conference, number AIAA 69-243, Williamsburg, VA, 1969. March 3-5.

[64] G.L. Cann, R.L. Harder, and S.T. Nelson. Experimental performance of the ALPHA thrustor. In *AIAA Electric Propulsion and Plasmadynamics Conference*, number AIAA 67-687, Colorado Springs, Colorado, 1967. September 11–13.

[65] T. Yoshikawa, Y. Kagaya, Y. Yokoi, and H. Tahara. Performance characteristics of quasi-steady MPD thrusters. In *17th International Electric Propulsion Conference*, number IEPC 84-058, Tokyo, Japan, 1984. May 28-31.

[66] V. Kim, V. Tikhonov, and S. Semenikhin. The first quarterly report on the stages# 3a of the contract on the research studies NASW-4851 between RIAME MAI and NASA. Technical report, RIAME, Moscow Aviation Institute, Moscow, Russia, April 1996.

[67] S. Bennett, G. Enos, R John, and W. Powers. Magnetoplasmadynamic thrustor research. Technical Report NAS 3-8907, Avco Missiles, Space and Electronics Group; Space Systems Division, Lowell, MA, May 1967.

[68] V.B. Tikhonov, S.A. Semenihin, V.A. Alexandrov, G.A. Dyakonov, and G.A. Popov. Research of plasma acceleration processes in self-field and applied magnetic field thrusters. In 23^{rd} *International Electric Propulsion Conference*, Seattle, WA, USA, 1993. IEPC-93-076.

[69] V.V. Zhurin, A.G. Popov, A.A. Porotnikov, V.B. Tikhonov, and Yu.A. Utkin. The state of research and development of end-hall plasma thrusters in the USSR. In 22^{nd} *International Electric Propulsion Conference*, number IEPC-91-080, Viareggo, Italy, 1991. October 14-17.

[70] V. Kim, V. Tikhonov, and S. Semenikhin. The third quarterly report on the stages # 5 - 6 of the contract on the research studies NASW-4851 between RIAME MAI and NASA. Technical report, RIAME, Moscow Aviation Institute, Moscow, Russia, June 1995.

[71] Roger M. Myers, David Wehrle, Mark Vernyi, Jim Biaglow, and Shawn Reese. A preliminary characterization of applied-field MPD thruster plumes. In *AIAA/SAE/ASME/ASEE 27th Joint Propulsion Conference and Exhibit*, number AIAA-91-2339, Sacramento, CA, USA, 1991. June 24-27.